Hausdorff Distance-based Tool Position Planning Method for Plunge Milling of 3D Impeller Channels in Shroud-enabled Blade Milling

yang Min Chen
Lei Dong
dongleishdj@126.com

Shanghai Dianji University

Research Article

Keywords: 3D impeller channel plunge milling, minimum unidirectional Hausdorff distance, tool pose and position optimisation, numerical example, reduced allowance and improved its uniformity

Posted Date: April 1st, 2025

DOI: https://doi.org/10.21203/rs.3.rs-6274183/v1

Hausdorff Distance-based Tool Position Planning Method for Plunge Milling of 3D Impeller Channels in Shroud-enabled Blade Milling

Chen Min yang, Shanghai DianJi university, 300 Shui Hua Rd., Shanghai 201306, People's Republic of China, Email: 15051137987@163.com, Fax: +8602138226253, Tel: +8615051137987

Dong Lei*, Shanghai DianJi university, 300 Shui Hua Rd., Shanghai 201306, People's Republic of China, Email: dongleishdj@126.com, Fax: +8602138226253, Tel: +8613918511632

Abstract: In the context of plunge milling for rough-machined three-dimensional (3D) impeller channels using the shroud-enabled blade milling method, substantial non-uniform allowances often persist on the inner surface of the shroud. To address this issue, in the present study, a tool pose and position optimisation method based on the Hausdorff distance was proposed. A mathematical model was developed to optimise the initial pose and position of a flat-bottomed tool by minimising the unidirectional Hausdorff distance from its bottom plane to the inner surface of the shroud. This optimisation ensures that the allowance on the inner surface of the shroud after plunge milling is both minimal and uniformly distributed. Numerical simulations demonstrate that the proposed method reduced the mean absolute error by 57.79% and significantly enhanced the uniformity of the error distribution, thereby verifying its effectiveness in improving machining accuracy.

Keywords: 3D impeller channel plunge milling; minimum unidirectional Hausdorff distance; tool pose and position optimisation; numerical example; reduced allowance and improved its uniformity

0 Introduction

Centrifugal compressors are extensively utilised across various industries, including air separation, metallurgy, petrochemicals, aerospace, and natural gas transportation. The machining efficiency and precision of their core component, the three-dimensional (3D) impeller, have attracted significant attention from researchers worldwide. The accuracy of impeller machining is primarily determined by the precision of the blade's curved surface fabrication. Since the blade's curved surface is often designed as a non-developable ruled surface, it is typically machined using one-pass side milling with cylindrical or conical tools. A key research focus in the field of CNC machining for complex curved surfaces is improving the side milling accuracy of these tools to ensure that the tool envelope closely approximates the blade's curved surface. Simultaneously, reducing algorithmic complexity to enhance computational efficiency and stability remains a crucial challenge in advancing high-precision machining techniques. Tool position planning methods can be roughly divided into five categories: the direct offset method[1-2], the local high-order tangential contact method[3-5], the multi-tangential point method[6-8], the tool envelope method[9-10], and the single-tool position optimisation method[11-12]. In the machining process of the impeller from blank to finished product, approximately 60-90% of the material is removed[13], the vast majority of which is removed in rough machining. In addition, most of the impeller materials, such as titanium alloys, stainless steel, and high-temperature alloys, are difficult to machine and undergo significant work hardening during processing. As a result, in industrial settings, the low machining efficiency of impellers often leads to delays in overall product

manufacturing, causing severe imbalances in production schedules. As such, improving impeller machining efficiency has become the primary objective for impeller manufacturing enterprises. At present, three main rough machining methods are employed for impellers: five-axis side milling, linear axis linkage high-speed milling, and plunge milling. In the early days, impellers were usually side milled in layers on five-axis machining centres[14-15], with low machining efficiency and high machining costs[16]. When the linear axis linkage machining method is used[17-19], the two rotary axes of the five-axis machine are fixed, and only three linear axes are used for linkage machining, resulting in better machining stability and a significant increase in machining efficiency. In the plunge milling method, the tool primarily experiences axial forces during machining. Since the axial stiffness of the tool is significantly higher than its radial stiffness, this method offers improved stability and cutting performance. As a result, plunge milling has garnered widespread attention for its application in the rough machining of impeller-type components. For rough plunge machining of the centrifugal 3D impeller channel, the fixed-axis method or variable-axis plunge machining method is typically used[20-22]. The fixed-axis plunge milling method offers greater stability; however, it results in non-uniform machining allowances, necessitating additional semi-finishing processes before the final blade finishing stage. In contrast, the variable-axis plunge milling method, while slightly less stable, provides a more uniform allowance near the blade after machining, making it the preferred choice in many applications. In the impeller machining process, if the traditional hub-blade milling method is used, the blades are first milled on the hub and then welded to the turned shroud. However, since the inner surface of the shroud is a positively curved surface, this approach increases the risk of blade root weld edge bending deformation and the likelihood of interface defects[23], including weld cracking. The shroud-enabled blade milling method can effectively alleviate the weld cracking by milling the blade on the shroud and then welding it to the hub. This is because the inner surface of the hub has a negatively curved geometry. Nevertheless, regarding the rough plunge milling method[24], which offers high machining efficiency, a key challenge arises in approximating the inner surface of the shroud, particularly when it has a positive curvature, using the bottom plane of a flat-bottomed tool. Conventional tool position planning methods often result in large and uneven machining allowances. To address this issue, a tool pose and position optimisation model was proposed in the present study. The proposed model minimises the unidirectional Hausdorff distance from the tool's bottom plane to the inner surface of the shroud. This optimisation ensures a minimal and uniform allowance after machining.

1 Best consistent approximation model for the bottom plane of a flat-bottomed tool approximating the inner surface of the shroud

1.1 Best consistent approximation model

The unidirectional Hausdorff is able to characterise the maximum deviation of one geometric object with respect to another geometric object, which is expressed below:

$$h(A,B)=\max_{a\in A}\min_{u,v\in B}\|a-b\| \tag{1}$$

In order to make the bottom plane of the flat-bottomed tool as close as possible to the inner surface of the impeller shroud, the bottom plane of the tool is set to A, which is discretised to obtain the point set $P\{p_1,p_2\ldots,p_n\}$, and the inner surface of the impeller shroud is set to B. The normal projection of each point in the point set $P\{p_1,p_2\ldots,p_n\}$ to the respective corresponding curved surface B yields the mapped point set $Q\{q_1,q_2,\ \ldots,q_n\}$. When the points $p_i(i=1,\cdots,n)$

in the point set P correspond to the points $q_i(i = 1, \cdots, n)$ in the point set Q one-to-one, $\max_{i=1,\cdots,n} d(p_i - q_i)$ represents the unidirectional Hausdorff distance from the bottom plane of the tool to the inner surface of the shroud. The objective is to minimise this distance, meaning that the largest of the minimum distances from all points on the bottom plane of the tool to the inner surface of the shroud is minimised. The corresponding planning model is expressed as follows:

$$\begin{aligned} &\min_{\boldsymbol{x}} \quad h \\ &s.t. \;\; d_i(P(p_i, \boldsymbol{x}), Q(q_i, \boldsymbol{x})) - h \le 0 \quad i = 1,2,\ldots,n \end{aligned} \tag{2}$$

where h is the characteristic parameter, which represents the objective function of the optimisation model, and its actual meaning is the unidirectional Hausdorff distance from the discrete point $p_i(i = 1, \cdots, n)$ on the bottom surface of the tool A to the inner surface of the shroud; $d_i(P(p_i, \boldsymbol{x}), Q(q_i, \boldsymbol{x}))$ denotes the minimum distance from the discrete point p_i on the bottom surface A of the tool to the inner surface of the shroud after a rotation and translation change; $x = (\alpha, \beta, \gamma, t)$ is the similar transformation parameter, where α、β、γ are the rotation angles of the tool around the x-axis, y-axis and z-axis, respectively, and t is the vertical travel distance of the tool along the z-axis; and $(h, x) = (h, \alpha, \beta, \gamma, t)$ is the optimisation variable of the planning model.

1.2 Solution of mapping points

The inner surface of the shroud of the impeller is obtained by rotating the curve C_P^S or C_S^S in the shroud around the rotary axis Z of the impeller, and the vector equation is expressed as follows:

$$S_s\text{:}\;\; \mathbf{S}_s = \mathbf{S}_s(u, \theta) = \mathbf{B}(\theta)\mathbf{C}(u) \tag{3}$$

where $B(\theta) = \begin{bmatrix} \cos\theta & -\sin\theta & 0 \\ \sin\theta & \cos\theta & 0 \\ 0 & 0 & 1 \end{bmatrix}$ is the group of rotations around the impeller rotary axis Z; and θ is the rotation angle of the rotations around the axis Z. When $\mathbf{C}(u)$ is set to the parametric equation of the c_p^S curve and $u \in [0,1]$ is its parameter, then the coordinate equation of the inner surface of the shroud can be expressed as follows:

$$S(u, \theta) = \begin{cases} x_\theta(u) = x(u)\cos\theta - y(u)\sin\theta \\ y_\theta(u) = x(u)\sin\theta + y(u)\cos\theta \\ z_\theta(u) = z(u) \end{cases} \tag{4}$$

where $x(u), y(u), z(u)$ are the coordinate values of the points on the curve c_p^S. Regarding the point $p_i = (x_i, y_i, z_i)$ $(i = 1, 2, \cdots, n)$, the coordinates of its mapping point $q_i = (x(u), y(u), z(u))$ $(i = 1, 2, \cdots, n)$ to the inner surface of the shroud are determined by the parameters u and θ only. The formula for the distance between two points obtained from the distance squared function can be expressed as follows:

$$d(u, \theta) = \sqrt{[x_\theta(u) - x_i]^2 + [y_\theta(u) - y_i]^2 + [z_\theta(u) - z_i]^2} \tag{5}$$

After fixing the parameter u, minimising $d(u,\theta)$ is equivalent to optimising the rotation angle θ. If θ is derived and made zero, the optimal rotation angle θ^{opt} should conform to the following equation:

$$\cos\theta^{opt} = \frac{x(u)\cdot x_i + y(u)\cdot y_i}{\sqrt{\left[x(u)^2 + y(u)^2\right]\cdot(x_i^2 + y_i^2)}} \tag{6}$$

Substituting Equations (4) and (6) into Equation (5) yields the univariate function:

$$d(u) = \sqrt{\left(\sqrt{x(u)^2+y(u)^2} - \sqrt{x_i^2 + y_i^2}\right)^2 + \left(z(u) - z_i\right)^2} \tag{7}$$

The final optimisation objective is transformed into a minimisation issue for a univariate function. As shown in

, the minimum distance parameter u_{min} can be solved efficiently using the iterative method.

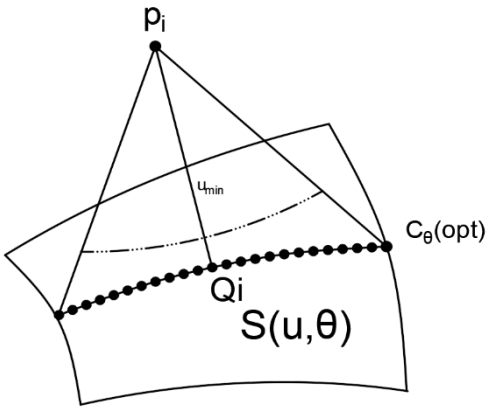

Fig.1 Solution of mapping points

$$u_{min} = arg\min_{u} d(u) \tag{8}$$

After determining u_{min}, the coordinates of the mapping point q_i are:

$$q_i = S(u_{min}, \theta^{opt}) = \left(x_{\theta^{opt}}(u_{min}), y_{\theta^{opt}}(u_{min}), z(u_{min})\right)$$

1.3 Linearised solution of the model

The key to solving for the minimum unidirectional Hausdorff distance from the discrete point set p_i on the bottom surface of the flat-bottomed tool to the inner surface of the shroud is the linearisation of the nonlinear constraint $d_i(P(p_i, \boldsymbol{x}), Q(q_i)) \leq h \leq$h. If $d_i(P(p_i, \boldsymbol{x}), Q(q_i))$ is Taylor-expanded at the zero point $x_0 = (\alpha_0, \beta_0, \gamma_0)$ of the parametric transformation by omitting the second-order and higher-order minors, the following can be obtained:

$$d_i(x) \approx d_i(x_0) + \nabla d_i(x_0) * \Delta x \tag{9}$$

where $\nabla d_i(x_0) = \left[\frac{\partial d_i}{\partial \alpha}, \frac{\partial d_i}{\partial \beta}, \frac{\partial d_i}{\partial \gamma}, \frac{\partial d_i}{\partial t}\right]_{x=x_0}$ characterises the sensitivity of the pose and position adjustment; and $\Delta x = (\Delta\alpha, \Delta\beta, \Delta\gamma, \Delta t)$ is the incremental parameter. The constraint $d_i(x_0) + \nabla d_i(x_0) * \Delta x \leq h$ is transformed into a linear planning issue by introducing the relaxation variable $s_i \geq 0$. The simplex or interior point method is utilised to solve for the increment Δx, and the pose and position $x_{k+1} = x_k + \eta \Delta x$ is iteratively updated, where the step size $\eta \in (0,1]$, until the convergence condition of the incremental norm $\|\Delta x\| < \varepsilon$ or the change in the objective value $|h_{k+1} - h_k| < \epsilon$, or the maximum number of iterations N_{max} has been reached.

2 Determination of initial tool position at the time of plunge milling of rough machined 3D impeller channels when the shroud-enabled blade milling method is used

The fundamental principle of rough machining is to maximise material removal efficiency while maintaining process stability. In practical applications, it is essential to ensure that the tool diameter remains smaller than the minimum distance L_{min} between two adjacent blades to prevent interference. Since the impeller gas channel usually shows a trend of gradual increase from the inlet to the outlet, the triangular tool traveling method was adopted for tool path planning to minimise the number of tool lifts, thereby enhancing machining efficiency and reducing unnecessary interruptions in the cutting process.

2.1 Calculation of minimum distance $\boldsymbol{L_{min}}$

The minimum distance L_{min} can be approximated using the following equation,

$$L_{min} \approx \min_{1<k<n} \left(\frac{2\pi R_k - N m_k}{2N}\right) \tag{10}$$

where n is the number of data points of the blade root; R_k is the radius of the impeller at

the k^{th} data point; m_k is the thickness of the blade at the k^{th} data point; and N is the number of blades.

2.2 Determination of maximum tool radius $\boldsymbol{r_{max}}$

Considering the machining allowance δ and avoiding interference, a safeguard factor μ is introduced, which is usually $(1.2 < \mu < 1.5)$. The final maximum tool radius is:

$$r_{max} = \frac{L_{min} - 2\delta}{2 * \mu} \tag{11}$$

2.3 Calculation of step $\Delta \boldsymbol{l}$ for grooving

Grooving plays a crucial role in reducing machining stress during the impeller manufacturing process and serves as a preparatory step for subsequent groove expansion. To implement this, the machining area curves C_{ps}'' and C_{ss}'' are discretised into corresponding point sets O_{ps}^{i} $(i = 1, 2, \cdots, n)$ and O_{ss}^{i} $(i = 1, 2, \cdots, n)$, as shown in Figure 2. The midpoint set O_i $(i = 1, 2, \cdots, n)$ of the corresponding points is obtained in order and each point set is connected to form the grooving tool position points. The machining step Δl is obtained according to the curvature k_i of the curve and can be expressed as follows:

$$\Delta l = 2\left[\left(\frac{1}{k_i}\right)^2 - \left(\frac{1}{k_i} - \epsilon\right)^2\right]^{0.5} \tag{12}$$

where ϵ is the permissible machining error.

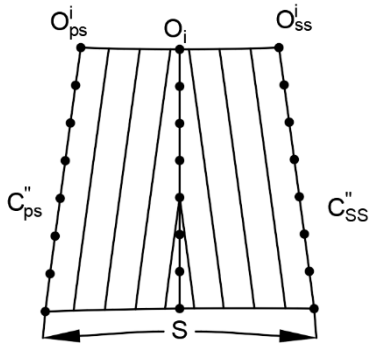

Fig.2 Triangular tool traveling method

2.4 Determination of the number of travelled lines and grooving paths

If the arc length of the inner surface of the shroud in the machining area on the outlet side is S, the permissible thickness allowance limit of the inner surface of the shroud in the depth direction on the outlet side is h, and the radius of the flat-bottomed tool is r, then the number of traveled lines N_{V1} is:

$$N_{V1} = \frac{S}{2\sqrt{2r * h}} \tag{13}$$

Grooving is implemented using the triangular tool traveling method. As shown in **Error! Reference source not found.** 3, the line from A_i to $\boldsymbol{C_i}$ $(i = 1, \ldots, n)$ is the groove expansion line, B_j $(j = 1,2, \ldots, m)$ is the intersection of A_i to $\boldsymbol{C_i}$, the machining order is $A_i \rightarrow B_j \rightarrow \boldsymbol{C_i}$, and the number of extended grooves is N_{V1}.

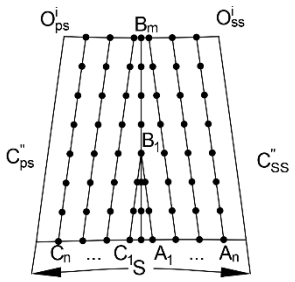

Fig.3 Tool planning using the triangular tool traveling method

By means of the described method, the tool path can be effectively planned to reduce the number of tool lifts in the machining process and improve the machining efficiency.

3 Numerical value example

To validate the effectiveness of the proposed Hausdorff distance-based tool position optimisation method for plunge milling in three-dimensional impeller channels under the shroud-enabled blade milling method, an actual impeller was selected for testing. The impeller had eight blades, an outer diameter of 706 mm, an impeller channel width ranging from 192 mm to 280 mm, a blade inlet height of 80.7 mm, and an outlet height of 40.8 mm. The initial tool plunge milling position was planned and optimised using the proposed model. Figure 4 illustrates the impeller used in the experiment.

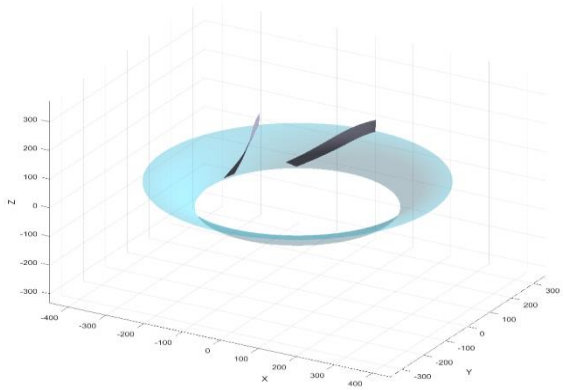

Fig.4 Shroud surface and corresponding blades

3.1 Analysis of the optimisation effect of the overall tool position

Considering the significant curvature variations of the shroud surface, the parameters for the first round of optimisation were set as follows: the rotation angle range was $[-0.1\pi, 0.1\pi]$, and the translation amount along the Z-axis was $[0, 2\ mm]$. The Hausdorff distance optimisation results shown in Figure 5 indicate that the minimum unidirectional Hausdorff distance from the bottom plane of the tool to the inner surface of the shroud (hereinafter referred to as the minimum unidirectional Hausdorff distance) was reduced by an average of 58.7% during the channel machining process for all the 82 tool positions, which verifies the overall effectiveness of the algorithm. Notably, the 43rd tool position exhibited a negative optimisation effect of 18.4%. The specific causes of this anomaly and potential solutions were analysed in the subsequent single tool position evaluation.

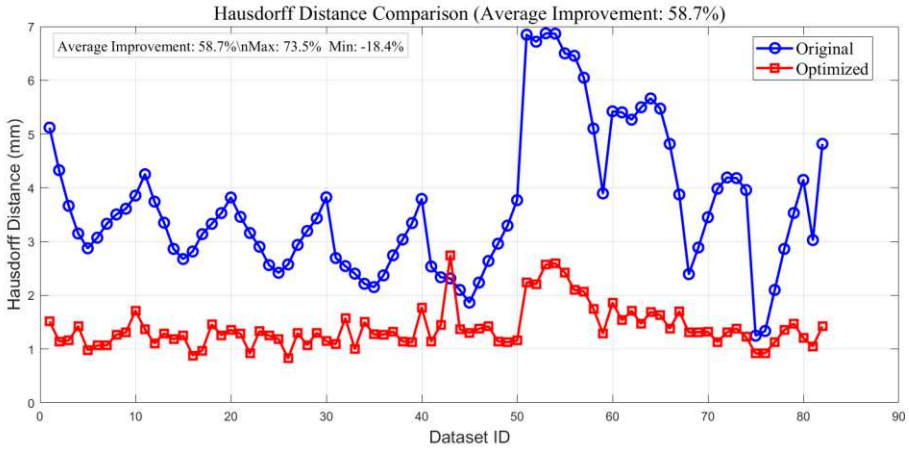

Fig.5 Overall tool position optimisation effect

The minimum unidirectional Hausdorff distance reduction ratio alone does not intuitively reflect the machining effect. Figure 6(a) illustrates the optimisation effect of the direct distance, defined as the distance between the set of tool position points and the corresponding set of points on the surface to be machined (i.e., the set of mapping points), across all 82 tool positions. After optimisation, the overall direct distance was reduced by 57.09%, and the uniformity of error distribution was significantly improved. As shown in Figure 6(b), statistical analysis reveals that before optimisation, 14.8% of the direct distances were less than 0.5 mm, and 41.2% were less than 1 mm. After optimisation, these proportions increased to 35.3% and 91%, respectively, effectively preventing both excessive and insufficient cutting. These improvements demonstrate the robustness of the proposed algorithm.

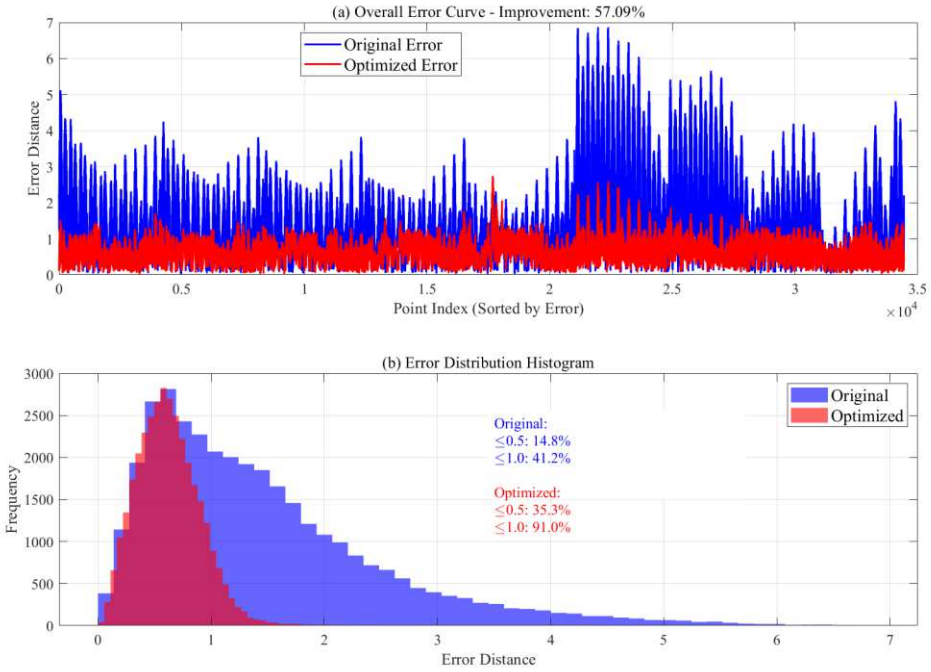

Fig.6 Error improvement magnitude

3.2 Secondary optimisation of single tool position

As shown in Figure 5 and Figure 6, the optimisation of the 43rd tool position during machining was not ideal. To investigate the cause, its individual error was analysed separately.

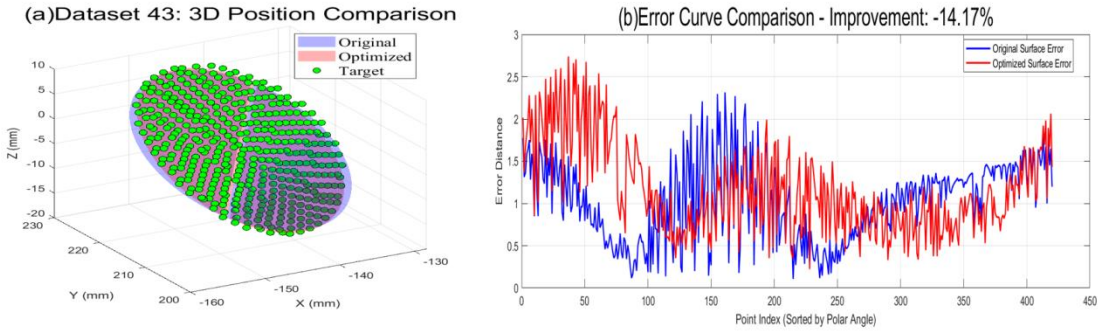

Fig.7 Analysis of the 43rd tool position

Regarding the abnormality observed at the 43rd tool position, local error analysis in Figure 7 reveals that the excessively close distance distribution between the initial tool position point set and the target curved surface results in unsatisfactory optimisation outcomes. To address this issue, the rotation parameter range was tightened to $[-0.05\pi, 0.05\pi]$, refining the optimisation process. After implementing this secondary optimisation, the error at the 43rd tool position improved by 43.45%, as shown in Figure 8. The adaptive adjustment of parameter ranges enhanced the algorithm's capability to identify the optimal solution at a

micro-scale level, leading to an improved alignment of the tool with the target curved surface.

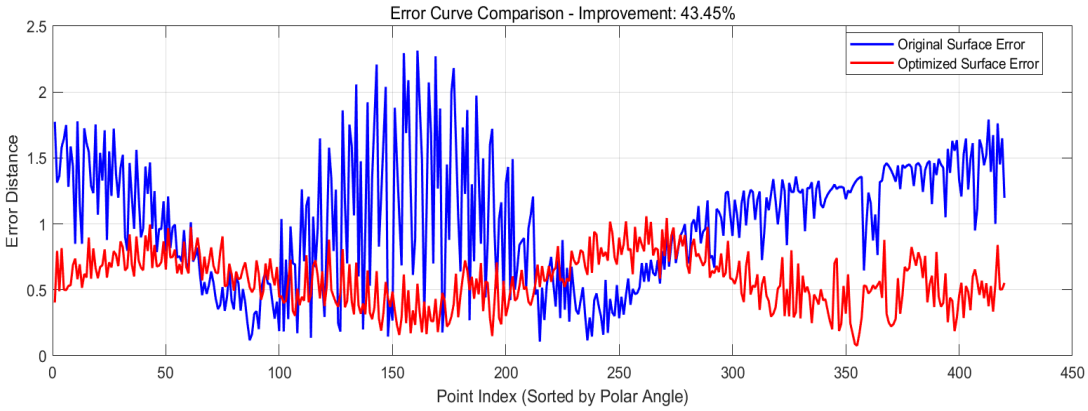

Fig.8 Secondary optimisation of the 43rd tool position

3.3 Comprehensive analysis of optimisation effect

By replacing the original 43rd tool position with the version that underwent secondary optimisation, a comparative visualisation of the overall tool envelope before and after optimisation is obtained, as shown in Figure 9. Figure 9(a) illustrates the tool envelope at the initial tool position, while Figure 9(b) presents the tool envelope at the optimised tool position. After two rounds of optimisation, the tool envelope at the optimised position exhibited a significantly improved fit with the target curved surface, effectively eliminating excessive cutting.

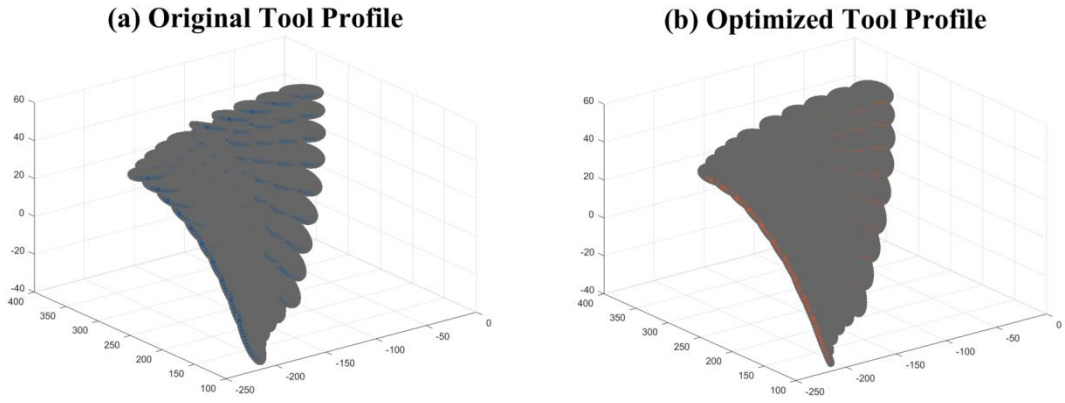

Fig.9 Initial tool position envelope vs. optimised tool position envelope

As shown in Figure 10, the error range of the initial tool position point set was -5.28 mm to 6.87 mm, while the error range of the optimised tool position was reduced to 0.00 mm to 2.68 mm. The mean absolute error μ was 1.30 mm before optimisation, and was reduced to 0.5487 mm after optimisation, which represents a reduction of 57.79%. The standard deviation σ decreased from 0.96 mm to 0.4 mm, which represents a reduction of approximately 41.7%, with improved concentration of error distribution.

$$\mu = \frac{1}{N}\sum_{i=1}^{N} \left|z_i - z_{target}\right| \tag{14}$$

$$\sigma = \sqrt{\frac{1}{N}\sum_{i=1}^{N} \left(\left|z_i - z_{target}\right| - \mu\right)^2} \tag{15}$$

where z_i is the actual tool height and z_{target} is the target height.

After adjustment, the average fitting accuracy between the tool and the machining surface was significantly improved, the overall fitting effect was better, the fluctuation of the error was reduced, and the fitting stability between the tool and the machining surface was enhanced.

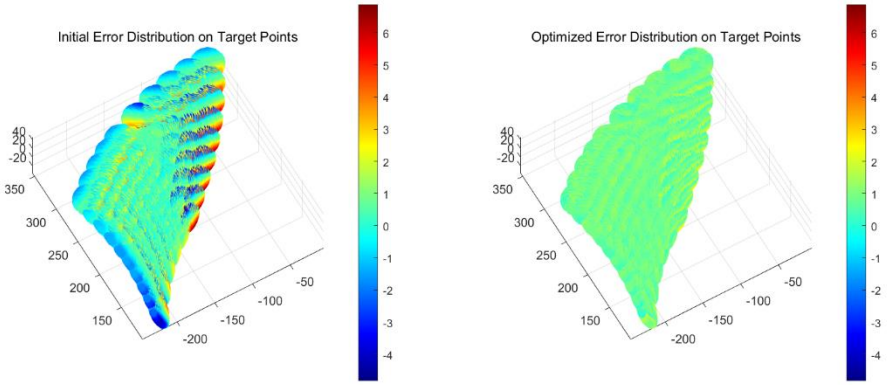

(a) Distribution of error of initial tool position (b) Distribution of error of optimised tool position

Fig.10 Distribution of errors of initial and optimised tool positions

4 Conclusion

In the present study, a best consistent approximation model was proposed for optimising the bottom plane of a flat-bottomed tool to approximate the inner surface of the impeller shroud. The solution method for determining the mapping points in the model and the linearised solution approach for the overall model were presented. This model was applied to optimise the initial tool position during the rough machining process of variable-axis plunge milling in the shroud-enabled blade milling method on an actual three-dimensional impeller. The optimisation results demonstrate that the overall tool position error was reduced by 57.09% compared to the initial positioning. Additionally, after optimisation, the error range of the point set decreased from -5.28 mm to 6.87 mm before optimisation to 0.00 mm to 2.68 mm. The mean absolute error was reduced from 1.30 mm to 0.5487 mm, representing a reduction of 57.79%.

Declaration

Funding: This work was supported by Natural Science Foundation of Shanghai, and the Award Number is 15ZR1417200.

Conflicts of interest: We declare that we do not have any commercial or associative interest that represents a conflict of interest in connection with the work submitted.

Availability of data and material: Not applicable

Code availability: Not applicable

Authors' contributions: Improve processing efficiency and machining precision of centrifugal 3D impeller

Ethics approval: Not applicable

Consent to participate: Yes

Consent for publication: Yes

References

1. Liu XW (1995) Five-axis NC cylindrical milling of sculptured surfaces. Comput Aided Des 27(12):887-894. https://doi.org/10.1016/0010-4485(95)00005-4
2. Hu DF, Chu ZK, Wu PL (2021) The control of machining errors of tool path for unequal diameter flank milling of globoidal cam. Int J Adv Manuf Technol, 113:2999-3009. https://doi.org/10.1007/s00170-021-06783-3
3. Gong H, Fang FZ, Hu XT, Cao LX, Liu J (2010) Optimization of tool positions locally based on the BCELTP for 5-axis machining of free-form surfaces. Comput Aided Des 42(6): 558-570. https://doi.org/10.1016/j.cad.2010.02.006
4. Zhu LM, Ding H, Xiong YL (2010) Third-order point contact approach for five-axis sculptured surface machining using non-ball-end tools (I): Third-order approximation of tool envelope surface. Sci China Tech Sci 53: 1904−1912. https://doi.org/10.1016/S1875-5372(10)60130-0
5. Zhu LM, Ding H, Xiong YL (2010) Third-order point contact approach for five-axis sculptured surface machining using non-ball-end tools (II): Tool positioning strategy. Sci China Tech Sci 53: 2190−2197
6. Bedi S, Mann S, Menzel C (2003) Flank milling with flat end cutters. Comput Aided Des 35(3):293-300. https://doi.org/10.1016/S0010-4485(01)00213-5
7. Menzel C, Bedi S, Mann S (2004) Triple tangent flank milling of ruled surfaces. Comput Aided Des 36(3):289-296. https://doi.org/10.1016/S0010-4485(03)00118-0
8. Senatore J, Moniès F, Redonnet JM, Rubio W (2005) Analysis of improved positioning in five-axis ruled surface milling using envelope surface. Comput Aided Des 37(10):989-998. https://doi.org/10.1016/j.cad.2004.09.00
9. Zhu LM, Zheng G, Ding H, Xiong YL (2010) Global optimization of tool path for five-axis flank milling with a conical cutter. Comput Aided Des 42(10): 903-910. https://doi.org/ 10.1016/j.cad.2010.06.005
10. Kong S, Yan YC, Zhang LQ, Feng QQ (2021) Cutter position optimization with tool runout for flank milling of non-developable ruled surfaces. Int J Adv Manuf Technol 115:2747–2763. https://doi.org/10.1007/s00170-021-07270-5
11. Yao CL, He GY, Ma WK, Yan YC, Wang ST, Yue C (2023) A finishing toolpath generation strategy for flank milling of ruled surface based on a Double-Point-Mirror method. Int J Adv Manuf Technol 129:3185–3195. https://doi.org/10.1007/s00170-023-12421-x
12. Dong L (2023) Positioning of a conical cutter for centrifugal blade finish machining

based on the best uniform approximation (BUA) method. Int J Adv Manuf Technol 127:3209–3219. https://doi.org/1001-3997(2024)07-0301-04

13. Dong L, Cao LX (2014) Research on the approximating method of tunnel surface with general cylindrical surface and its application in the plunge milling of impeller. Chin J Aero, 35(8):2331-2340. https://doi.org/10.7527/S1000-6893.2013.0436
14. Lim P (2009) Optimization of the rough cutting factors of impeller with five-axis machine using response surface methodology. Int J Adv Manuf Technol 45(7-8): 821-829. https://doi.org/10.1007/s00170-009-2011-1
15. Chuang LC, Young HT. (2007) Integrated rough machining methodology for centrifugal impeller manufacturing. Int J Adv Manuf Technol 34 (11-12):1062–1071. https://doi.org/10.1007/s00170-006-0675-3
16. Dong L, Chen MY (2024) A comparative experimental study on the rough machining methods of centrifugal three-dimensional impellers. Advances in Mechanical Engineering16(4): 1–17. https://doi.org/10.1177/16878132241244923
17. Heo EY, Kim DW, Kim BH, Jang DK, Chen FF. Chen. Efficient rough-cut plan for machining an impeller with a 5-axis NC machine. Int J Comput Int Manuf 21(8):971–983. https://doi.org/10.1080/09511920802010761
18. Pei LQ, Wei GJ, Bi HB (2013) Study of linear axes milling method in 3Dimpeller. Chin J Turbo, 2013,(2):49-51. https://doi.org/1006-8155（2013）02-0049-03
19. Han FY，Zhang DH，Wu BH，Luo M, Zhang XD (2015) High-efficiency section-by section slotting method for 4+1-axis NC machining of high-wrap impeller channel. Chin J Aero 2015,36 (5):1684–1694.
20. Ren JX, Tian WJ, Yao CF, Jiang ZN (2008) Experimental study on the overall structure of Titanium alloy with high-effect plunge milling process . Chin J of Mech Eng, 2008, (22): 2758-2761. https://doi.org/1004-132X(2008)22-2758-04
21. Liang Q，Wang YZ，Fu YH，Han ZY (2010) Key technologies in ruling surface impeller plunge milling. Chin J of Comput Int Manuf Sys 16(1):182 -187. https://doi.org/ 1006-5911(2010) 01-0182-0
22. Dong L Yang J Wang J(2024) Semi finish machining cutter location algorithm of variable axis plunge milling for ruled-surface impeller. Chin J Machinery Design & Manufacture 7:301–304. https://doi.org/10.1007/s00170-023-11706-5
23. Xiao X, Mao Y, Wang XC, Qin DQ, Fu L (2023) Effects of curvature direction on friction stir welding lap joint of aluminum alloy “S” curved surface. Int J Adv Manuf Technol 125:4693–4705. https://doi.org/10.1007/s00170-023-11043-7
24. Guo ML, Wang ZB, Wei ZC, Zhang ZH, He SL (2024) New plunge milling cutter and two-dimensional cavity process based on dislocation chip-separation principle. Int J Adv Manuf Technol 135:1551–1564. https://doi.org/10.1007/s00170-024-14609-1

Supplementary Files

This is a list of supplementary files associated with this preprint. Click to download.

- Acknowledgment.docx
- ConflictsofInterest.docx